

6399 Chapter 14

6400 Optical Elements and Keywords, Complements

6401 **Abstract** This chapter is not a review of the 60+ optical elements of zgoubi's
6402 library. They are described in the Users' Guide. One aim here is, regarding some of
6403 them, to briefly recall some aspects which may not be found in the Users' Guide and
6404 yet addressed, or referred to, in the theoretical reminder sections and in the exercises.
6405 This chapter is not a review of the 40+ monitoring and command keywords available
6406 in zgoubi, either. However it reviews some of the methods used, by keywords such
6407 as MATRIX (computation of transport coefficients from sets of rays), FAISCEAU
6408 (which produces beam emittance parameters), and others. This chapter in addition
6409 recalls the basics of transport and beam matrix methods, in particular it provides the
6410 first order transport matrix of several of the optical elements used in the exercises, in
6411 view essentially of comparisons with transport coefficients drawn from raytracing,
6412 in simulation exercises.

6413 14.1 Introduction

6414 Optical elements are the basic bricks of charged particle beam lines and accelerators.
6415 An optical element sequence is aimed at guiding the beam from one location to
6416 another while maintaining it confined in the vicinity of a reference optical axis.
6417 Zgoubi library offers a collection of about 100 keywords, amongst which about
6418 60 are optical elements, the others being commands (to trigger spin tracking, trigger
6419 synchrotron radiation, print out particle coordinates, compute beam parameters,
6420 etc.). This library has built over half a century, so it allows simulating most of
6421 the optical elements met in real life accelerator facilities. Quite often, elements
6422 available provide different ways to model a particular optical component. A bending
6423 magnet for instance can be simulated using AIMANT, or BEND, CYCLOTRON,
6424 DIPOLE[S][-M], FFAG, FFAG-SPI, MULTIPOL, QUADISEX, or a field map and
6425 TOSCA, CARTEMES or POLARMES to handle it. These various keywords have
6426 their respective subtleties, though, more on this can be found in the "Optical Elements
6427 Versus Keywords" Section of the guide [1, page 227], which tells "Which optical

6428 component can be simulated. Which keyword(s) can be used for that purpose”. For
 6429 a complete inventory of optical elements, refer to the “Glossary of Keywords” found
 6430 at the beginning of PART A [1, page 9] or PART B of the Users’ Guide [1, page 227].

6431 Optical elements in *zgoubi* are actually field models, or field modeling methods
 6432 such as reading and handling field maps. Their role is to provide the numerical
 6433 integrator with the necessary field vector(s) to push a particle further, and possibly
 6434 its spin, along a trajectory. The following sections introduce the analytical field
 6435 models which the simulation exercises resort to.

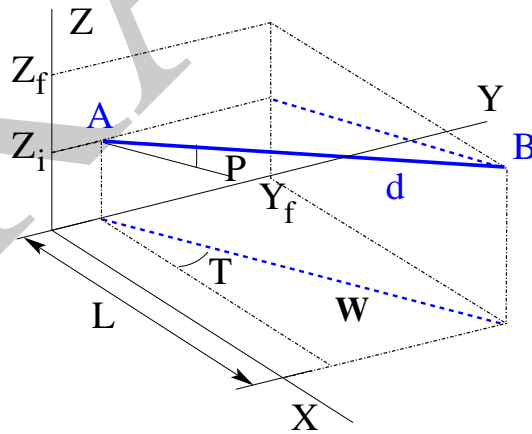
6436 *Zgoubi*’s coordinate nomenclature, as well as the Cartesian or cylindrical refer-
 6437 ence frames used in the optical elements and field maps, have been introduced in
 6438 Sect. 1.2 and Fig. 1.5.

6439 14.2 Drift Space

6440 This is the DRIFT, or ESL (for the French “ESpace Libre”) optical element, through
 6441 which a particle moves on a straight line. From the geometry and notations in
 6442 Fig. 14.1, with L the length of the drift, coordinate transport satisfies

$$\begin{cases} X_f - X_i = L \\ Y_f - Y_i = L \tan T \\ Z_f - Z_i = L \tan P / \cos T \\ \text{path length } d = L / (\cos T \cos P) \end{cases} \quad (14.1)$$

Fig. 14.1 An L -long drift in *zgoubi* ($O;X,Y,Z$) frame, with origin at the start of the drift. A particle flies from $A(Y_i, Z_i)$ to $B(Y_f, Z_f)$, at an angle P to the (X, Y) plane. Projection W of its straight path in (X, Y) plane is at an angle T to the X axis



6443 *Linear approach*

6444 Coordinate transport from initial to final position in the linear approximation is
 6445 written (with z standing indifferently for x or y , subscripts i for initial and f for final
 coordinates) (Fig. 14.2)

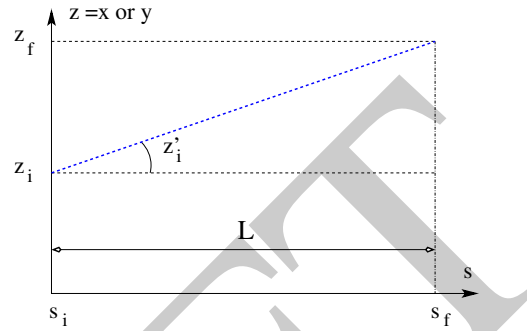


Fig. 14.2 A drift section with length $L = s_f - s_i$, and projection of a straight trajectory in the (s, z) plane, at an angle z' (standing for x' or y') to the s axis

6446

$$\begin{cases} z_f = z_i + L z'_i \\ z'_f = z'_i \\ \delta l_f - \delta l_i = \beta c \delta t = \frac{L}{\gamma^2} \frac{\delta p}{p} \\ \delta p_f / p = \delta p_i / p \end{cases} \quad \text{or, } T_{\text{drift}} = \begin{pmatrix} 1 & L & 0 & 0 & 0 & 0 \\ 0 & 1 & 0 & 0 & 0 & 0 \\ 0 & 0 & 1 & L & 0 & 0 \\ 0 & 0 & 0 & 1 & 0 & 0 \\ 0 & 0 & 0 & 0 & 1 & \frac{L}{\gamma^2} \\ 0 & 0 & 0 & 0 & 0 & 1 \end{pmatrix} \quad (14.2)$$

6447 where βc is the particle velocity, $p = \gamma m \beta c$ its momentum, γ is the Lorentz relativistic factor.
 6448

6449 **14.3 Guiding**

6450 Beam guiding is in general assured using dipole magnets to provide a uniform field,
 6451 normal to the bend plane. Gradient dipoles combine guiding and focusing in a single
 6452 magnet, this is the case in cyclotrons, this is also the case in some synchrotrons,
 6453 for instance the BNL AGS [2], the CERN PS [3]. By principle, FFAG dipoles have
 6454 pole faces shaped to provide a highly non-linear dipole field, $B \propto r^k$ (Sect. 10).
 6455 Dipole magnets sometimes include a sextupole component for the compensation of
 6456 chromatic aberrations [4]. Non-linear optical effects may be introduced by shaping
 6457 entrance and or exit EFBs, a parabola for instance for x^2 field integral dependence,
 6458 a cubic curve for x^3 dependence (see Chap. 13).

6459 Low energy beam guiding also uses electrostatic deflectors, shaped to provide a
 6460 field normal to the trajectory arc, and focusing properties. Plane condensers may be

6461 used for beam guiding as well. They are also used at higher energies for some special
6462 functions, such as pretzel orbit separation, extraction septa, etc.

6463 Guiding optical elements are dispersive systems: trajectory deflection has a first
6464 order dependence on particle momentum.

6465 14.3.1 Dipole Magnet, Curved

6466 This is the DIPOLE element (an evolution of the 1972's AIMANT [1]) or variants:
6467 DIPOLES, DIPOLE-M. Lines of constant field are isocentric circle arcs. The magnet
6468 reference curve is a particular arc, at a reference radius r_0 . The field in the median
6469 plane can be written

$$B_z(r, \theta) = \mathcal{G}(r, \theta) B_0 \left(1 + N \frac{r - r_0}{r_0} + N' \left(\frac{r - r_0}{r_0} \right)^2 + N'' \left(\frac{r - r_0}{r_0} \right)^3 + \dots \right) \quad (14.3)$$

6470 $N^{(n)} = d^n N / dY^n$ are the field index and derivatives. $\mathcal{G}(X)$ describes the longitudinal
6471 shape of the field, from a plateau value in the body to zero away from the magnet
6472 (Fig. 14.3). It can be written under the form

$$\mathcal{G}(X) = G_0 F(d(X)) \quad \text{with} \quad G_0 = \frac{B_0}{r_0^{n-1}} \quad (14.4)$$

6473 where B_0 is the field at pole tip at r_0 , and $F(d)$ a convenient model for the field
6474 fall-off, e.g. (the Enge model, Sect. 14.3.3),

$$F(d) = \frac{1}{1 + \exp[P(d)]}, \quad P(d) = C_0 + C_1 \left(\frac{d}{g} \right) + C_2 \left(\frac{d}{g} \right)^2 + C_3 \left(\frac{d}{g} \right)^3 + \dots \quad (14.5)$$

6475 with d (an X -dependent quantity) the distance from (X, Y, Z) location to the magnet
6476 EFB, g the characteristic extent of the field fall-off.

6477 Linear approach

6478 The first order transport matrix of a sector dipole with curvature radius ρ , deflection
6479 α and index n , in the hard-edge model, writes

$$T_{\text{bend}} = \begin{pmatrix} C_x & S_x & 0 & 0 & 0 & \frac{r_x^2}{\rho} (1 - C_x) \\ C'_x & S'_x & 0 & 0 & 0 & \frac{1}{\rho} S_x \\ 0 & 0 & C_y & S_y & 0 & 0 \\ 0 & 0 & C'_y & S'_y & 0 & 0 \\ \frac{1}{\rho} S_x & \frac{r_x^2}{\rho} (1 - C_x) & 0 & 0 & 1 & \frac{r_x^3}{\rho^2} (\rho \alpha - S_x) \\ 0 & 0 & 0 & 0 & 0 & 1 \end{pmatrix} \quad \text{with} \quad \begin{cases} C = \cos \frac{\rho \alpha}{r} \\ C' = \frac{dC}{ds} = \frac{1}{\rho} \frac{dC}{d\alpha} = \frac{-S}{r^2} \\ S = r \sin \frac{\rho \alpha}{r} \\ S' = \frac{dS}{ds} = \frac{1}{\rho} \frac{dS}{d\alpha} = C \\ (*)_x : r = \rho / \sqrt{1 - n} \\ (*)_y : r = \rho / \sqrt{n} \end{cases} \quad (14.6)$$

6480 or, explicitly,

$$T_{\text{bend}} = \begin{pmatrix} \cos \sqrt{1-n}\alpha & \frac{\rho}{\sqrt{1-n}} \sin \sqrt{1-n}\alpha & 0 & 0 & 0 & \frac{\rho}{1-n} (1 - \cos \sqrt{1-n}\alpha) \\ -\frac{\sqrt{1-n}}{\rho} \sin \sqrt{1-n}\alpha & \cos \sqrt{1-n}\alpha & 0 & 0 & 0 & \frac{1}{\sqrt{1-n}} \sin \sqrt{1-n}\alpha \\ 0 & 0 & \cos \sqrt{n}\alpha & \frac{\rho}{\sqrt{n}} \sin \sqrt{n}\alpha & 0 & 0 \\ 0 & 0 & -\frac{\sqrt{n}}{\rho} \sin \sqrt{n}\alpha & \cos \sqrt{n}\alpha & 0 & 0 \\ \frac{1}{\sqrt{1-n}} \sin \sqrt{1-n}\alpha & \frac{\rho}{1-n} (1 - \cos \sqrt{1-n}\alpha) & 0 & 0 & 1 & \frac{\rho}{(1-n)^{3/2}} (\sqrt{1-n}\alpha - \sin \sqrt{1-n}\alpha) \\ 0 & 0 & 0 & 0 & 0 & 1 \end{pmatrix} \quad (14.7)$$

6481 Cancel the index in the previous sector dipole, introduce a wedge angle ε at
6482 entrance and exit EFBs. The first order transport matrix, accounting for the entrance
6483 and exit EFB wedge focusing (see Sect. 14.4.1), writes

$$T_{\text{bend}} = \begin{pmatrix} \frac{\cos(\alpha-\varepsilon)}{\cos \varepsilon} & \frac{\rho \sin \alpha}{\cos \varepsilon} & 0 & 0 & 0 & \frac{\rho(1-\cos \alpha)}{\cos \varepsilon} \\ -\frac{\sin(\alpha-2\varepsilon)}{\rho \cos^2 \varepsilon} & \frac{\cos(\alpha-\varepsilon)}{\cos \varepsilon} & 0 & 0 & 0 & \frac{\sin(\alpha-\varepsilon)+\sin \varepsilon}{\cos \varepsilon} \\ 0 & 0 & 1 - \alpha \tan \varepsilon & \rho \alpha & 0 & 0 \\ 0 & 0 & -\frac{\tan \varepsilon}{\rho} (2 - \alpha \tan \varepsilon) & 1 - \alpha \tan \varepsilon & 0 & 0 \\ \sin \alpha & 0 & 0 & 0 & 1 & \rho(\alpha - \sin \alpha) \\ 0 & 0 & 0 & 0 & 0 & 1 \end{pmatrix} \quad (14.8)$$

6484

6485 14.3.2 Dipole Magnet, Straight

6486 This is the MULTIPOL element. Lines of constant field are straight lines. An early
6487 instance of a straight dipole magnet is the AGS main dipole (Fig. 9.2), which combines
6488 steering and focusing, and features in addition a noticeable sextupole component [5].
6489 The multipole components $B_n(X, Y, Z)$ [$n=1$ (dipole), 2 (quadrupole), 3 (sextupole),
6490 ...] in the Cartesian frame of the straight dipole derive, by differentiation, from the
6491 scalar potential

$$V_n(X, Y, Z) = (n!)^2 \left(\sum_{q=0}^{\infty} (-1)^q \frac{\mathcal{G}^{(2q)}(X)(Y^2 + Z^2)^q}{4^q q!(n+q)!} \right) \left(\sum_{m=0}^n \frac{\sin\left(\frac{m\pi}{2}\right) Y^{n-m} Z^m}{m!(n-m)!} \right) \quad (14.9)$$

6492 where $\mathcal{G}^{(2q)}(X) = d^{2q} \mathcal{G}(X) / dX^{2q}$. In the case of pure dipole field for instance

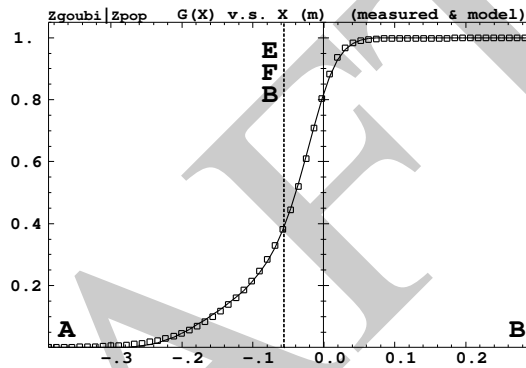
$$V_1(X, Y, Z) = \mathcal{G}(X) Z - \frac{\mathcal{G}''(X)}{8} (Y^2 + Z^2) + \frac{\mathcal{G}^{(4)}(X)}{512} (Y^2 + Z^2) Z \dots \quad (14.10)$$

6493 and

$$\begin{aligned}
 B_X(X, Y, Z) &= -\frac{\partial V_1}{\partial X} = \mathcal{G}'(X) Z - \frac{\mathcal{G}'''(X)}{8} (Y^2 + Z^2) \dots \\
 B_Y(X, Y, Z) &= -\frac{\partial V_1}{\partial Y} = -\frac{\mathcal{G}''(X)}{4} Y + \frac{\mathcal{G}^{(4)}(X)}{256} YZ \dots \\
 B_Z(X, Y, Z) &= -\frac{\partial V_1}{\partial Z} = \mathcal{G}'(X) - \frac{\mathcal{G}''(X)}{4} Z + \frac{3\mathcal{G}^{(4)}(X)}{512} Z^2 \dots \quad (14.11)
 \end{aligned}$$

6494 $\mathcal{G}(r, \theta)$ is a longitudinal form factor to account for the field fall-offs at the ends of the
 6495 magnet, modeled using Eq. 14.5, with distance d to the EFB in the latter, a function
 6496 of r and θ .

Fig. 14.3 Longitudinal field form factor (Eq. 14.4 - normalized to one) in BNL AGS main bend, taken along the magnet reference axis. Solid line: from Eq. 14.4 with g and C_i values from Eq. 14.14. Squares : measured field data. $X = 0$ is the origin in the field map frame, the vertical dashed line at $X_{\text{EFB}} = -5.62$ cm is the location of the EFB.



6497 14.3.3 Fringe Field, Modeling, Overlapping

6498 A fringe field model is described here, which is resorted to in several optical elements
 6499 of *zgoubi*'s library.

6500 Field shape at the EFBs of magnetic or electrostatic devices can be simulated
 6501 using a hard-edge model (the field is assumed to change following a Heaviside step).
 6502 When using stepwise ray-tracing techniques however, a smooth change of the field
 6503 can easily be accounted for. An efficient model is Enge's field form factor [6].

$$F(d) = \frac{1}{1 + \exp P(d)} \quad (14.12)$$

$$P(d) = C_0 + C_1 \left(\frac{d}{\lambda}\right) + C_2 \left(\frac{d}{\lambda}\right)^2 + C_3 \left(\frac{d}{\lambda}\right)^3 + C_4 \left(\frac{d}{\lambda}\right)^4 + C_5 \left(\frac{d}{\lambda}\right)^5$$

6504 where d is the distance to the field boundary and λ is the extent of the fall-off,
 6505 normally commensurate with gap aperture in a dipole, the radius at pole tip in a
 6506 quadrupole, etc.

6507 As an illustration, Fig. 14.3 shows $F(d)$ as matched to the measured end fields of
 6508 BNL AGS main magnet (Fig. 14.3) [7, 8], using

$$\lambda = \text{gap aperture} \approx 10 \text{ cm} \quad \text{and} \quad (14.13)$$

$$C_0 = 0.45473, C_1 = 2.4406, C_2 = -1.5088, C_3 = 0.7335, C_4 = C_5 = 0$$

6509 These C_i coefficient values result from an interpolation to measured field data, which
 6510 are also represented in the figure. The location of the EFB results from the following
 6511 constraint, which is part of the matching: the field integral on the down side of the
 6512 fall-off (the region from A to X=0 in Fig. 14.3) is equal to the complement to 1 of
 6513 the field integral on the rising side of the fall-off (X=0 to B region in the figure),
 6514 which writes

$$\int_{X_A}^{X_{\text{EFB}}} F(X) dX = \int_{X_{\text{EFB}}}^{X_B} dX - \int_{X_{\text{EFB}}}^B F(X) dX \Rightarrow X_{\text{EFB}} = X_B - \int_A^B F(X) dX \quad (14.14)$$

6515 A convenient property of this model is that changing the slope of the fall-off (*i.e.*,
 6516 changing λ) will not affect the location of the EFB.

6517 Inward fringe field extents may overlap when simulating an optical element
 6518 (Fig. 14.4). A way to ensure continuity of the resulting field form factor in such
 6519 case is to use

$$F = F_E + F_S - 1 \quad \text{or} \quad F = F_E * F_S \quad (14.15)$$

6520 where F_E (F_S) is the entrance (exit) form factor and follows Eq. 14.12. Both expres-
 6521 sions can be extended to more than two EFBs (for instance 4, to account for the 4
 6522 faces of a dipole magnet: entrance and exit faces, inner and outer radial boundaries).
 6523 Note that in that case of overlapping field extents, the field integral is affected, lower-
 6524 ing with more pronounced overlapping, it is therefore necessary to change the field
 6525 value (B_0 in Eq. 14.4 for instance) to recover the proper integrated strength.

6526 Overlapping Fringe Fields

6527 Zgoubi allows a superposition technique to simulate the field in a series of neighbor-
 6528 ing magnets. The method consists in computing the mid-plane field at any location
 6529 (R, θ) by adding individual contributions, namely [9]

$$B_Z(r, \theta) = \sum_{i=1, N} B_{Z,i}(r, \theta) = \sum_{i=1, N} B_{Z,0,i} \mathcal{F}_i(r, \theta) \mathcal{R}_i(r)$$

$$\frac{\partial^{k+l} \mathbf{B}_Z(r, \theta)}{\partial \theta^k \partial r^l} = \sum_{i=1, N} \frac{\partial^{k+l} \mathbf{B}_{Z,i}(r, \theta)}{\partial \theta^k \partial r^l} \quad (14.16)$$

6530 with $\mathcal{F}_i(r, \theta)$ and $\mathcal{R}_i(r)$ in each individual dipole in the series (Eqs. 10.7, 10.15).
 6531 Note that, in doing so it is not meant that field superposition would apply in reality
 6532 (FFAG magnets are closely spaced, cross-talk may occurs), however it appears to
 6533 allow closely reproducing magnet computation code outcomes.

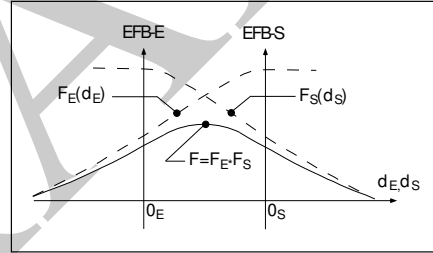
6534 Short Optical Elements

6535 In some cases, an optical element in which fringe fields are taken into account (of
 6536 any kind: dipole, multipole, electrostatic, etc.) may be given small enough a length,
 6537 L , that it finds itself in the configuration schemed in Fig. 14.4: the entrance and/or
 6538 the exit EFB field fall-off extends inward enough that it overlaps with the other EFB's
 6539 fall-off. In zgoubi notations, this happens if $L < X_E + X_S$. As a reminder [1]: in
 6540 the presence of fringe fields, X_E (resp. X_S) is the stepwise integration extent added
 6541 upstream (resp. added downstream) of the actual extent L of the optical element.

6542 In such case, zgoubi computes field and derivatives along the element using a
 6543 field form factor $F = F_E \times F_S$. F_E (respectively F_S) is the value of the Enge model
 6544 coefficient (Eq. 14.12) at distance d_E (resp. d_S) from the entrance (resp. exit) EFB.

6545 This may have the immediate effect, apparent in Fig. 14.4, that the integrated
 6546 field is not the expected value $B \times L$ from the input data L and B , and may require
 6547 adjusting (increasing) B so to recover the required BL .

Fig. 14.4 A sketch of overlapping entrance field form factor $F_E(d_E)$ (at the entrance "EFB-E") and exit $F_S(d_S)$ (at the exit "EFB-S"), and resulting form factor $F = F_E \times F_S$ accounted for in modeling the field within the optical element



6548 14.3.4 Toroidal Condenser

6549 This is the ELCYLDEF element in zgoubi. With proper parameters, it can be used
 6550 as a spherical, a toroidal or a cylindrical deflector.

Motion along the optical axis, an arc of a circle of radius r normal to electric field \mathbf{E} , satisfies

$$Er = v \frac{p}{q} = v(B\rho)$$

6551 with $p = mv$ the particle momentum, q its charge and $(B\rho) = p/q$ the particle
 6552 rigidity.

6553 The first order transport matrix of an electrostatic bend writes

$$T_{\text{condenser}} = \begin{pmatrix} C_x & S_x & 0 & 0 & 0 & \frac{2-\beta^2}{p_x^2} r_0 (1-C_x) \\ C'_x & S'_x & 0 & 0 & 0 & \frac{2-\beta^2}{r_0} S_x \\ 0 & 0 & C_y & S_y & 0 & 0 \\ 0 & 0 & C'_y & S'_y & 0 & 0 \\ -\frac{2-\beta^2}{r_0} S_x & -\frac{2-\beta^2}{p_x^2} r_0 (1-C_x) & 0 & 0 & 1 & r_0 \alpha \left[\frac{1}{\gamma^2} - \left(\frac{2-\beta^2}{p_x^2} \right)^2 \left(1 - \frac{S_x}{r_0 \alpha} \right) \right] \\ 0 & 0 & 0 & 0 & 0 & 1 \end{pmatrix} \quad (14.17)$$

with

$$\begin{cases} \alpha = \text{deflection angle} \\ C = \cos p\alpha \\ C' = \frac{dC}{ds} = -\frac{p^2}{r^2} S \\ S = \frac{r}{p} \sin p\alpha \\ S' = \frac{dS}{ds} = C \\ (*)_x : p = p_x = \sqrt{2 - \beta^2 - r_0/R_0} \\ (*)_y : p = p_y = \sqrt{r_0/R_0} \end{cases}$$

6554 14.4 Focusing

6555 Particle beams are maintained confined along a reference propagation axis by means
6556 of focusing techniques and devices. Methods available in zgoubi to simulate those
6557 are addressed here.

6558 14.4.1 Wedge Focusing

6559 Wedge focusing is sketched in Fig. 14.5. A wedge angle ε causes a particle at local
6560 excursion x to experience a change $\int B_y ds = x B_y \tan \varepsilon$ of the field integral compared
6561 the field integral through the sector magnet, thus in the linear approximation a change
6562 in trajectory angle

$$\Delta x' = \frac{1}{B\rho} \int B_y ds = x \frac{\tan \varepsilon}{\rho_0} \quad (14.18)$$

6563 with $B\rho$ the particle rigidity and ρ_0 its trajectory curvature radius in the field B_0
6564 of the dipole. Vertical focusing results from the non-zero off-mid plane radial field
6565 component B_x in the fringe field region (Fig. 14.7): from (Maxwell's equations)
6566 $\frac{\partial}{\partial y} \int B_x ds = \frac{\partial}{\partial x} \int B_y ds$ and Eq. 14.18 the change in trajectory angle comes out to
6567 be

$$\Delta y' = \frac{1}{B\rho} \int B_x ds = -y \frac{\tan \varepsilon}{\rho_0} \quad (14.19)$$

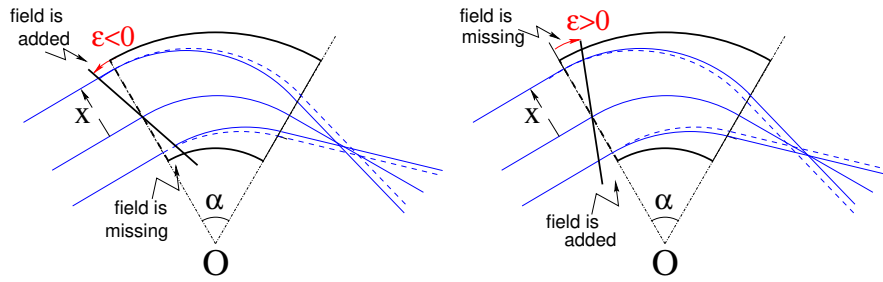


Fig. 14.5 Left: a focusing wedge ($\epsilon < 0$ by convention); opening the sector increases the horizontal focusing. Right: a defocusing wedge ($\epsilon > 0$); closing the sector decreases the horizontal focusing. The effect is the opposite in the vertical plane, opening/closing the sector decreases/increases the vertical focusing.

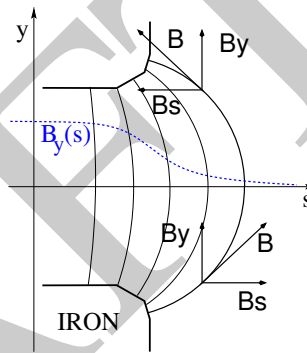


Fig. 14.6 Field components in the $B_y(s)$ fringe field region at a dipole EFB

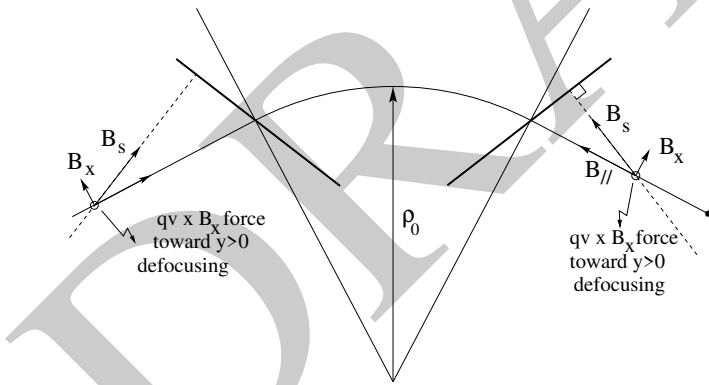


Fig. 14.7 Field components in the fringe field region at the ends of a dipole ($y > 0$, here, referring to Fig. 14.6). $B_{//}$ is parallel to the particle velocity. This configuration is vertically defocusing: a charged particle traveling off mid-plane is pulled away from the latter under the effect of $\mathbf{v} \times \mathbf{B}_x$ force component. Inspection of the $y < 0$ region gives the same result: the charge is pulled away from the median plane

6568 A first order correction ψ to the vertical kick accounts for the fringe field extent
6569 (it is a second order effect for the horizontal kick):

$$\Delta y' = -y \frac{\tan(\varepsilon - \psi)}{\rho_0} \quad (14.20)$$

6570 with

$$\psi = I_1 \frac{\lambda}{\rho_0} \frac{1 + \sin^2 \varepsilon}{\cos \varepsilon} \quad \text{with} \quad I_1 = \int_{\text{edge}} \frac{B(s)(B_0 - B(s))}{\lambda B_0^2} ds \quad (14.21)$$

6571 λ is the fringe field extent (Sect. 14.3.3), I_1 quantifies the flutter (see Sect. 4.2.1); a
6572 longer/shorter field fall-off (smaller/greater flutter) decreases/increases the vertical
6573 focusing.

6574 *Linear approach*

6575 A wedge focusing first order transport matrix writes

$$T_{\text{wedge}} = \begin{pmatrix} 1 & 0 & 0 & 0 & 0 & 0 \\ \frac{\tan \varepsilon}{\rho} & 1 & 0 & 0 & 0 & 0 \\ 0 & 0 & 1 & 0 & 0 & 0 \\ 0 & 0 & -\frac{\tan \varepsilon}{\rho} & 1 & 0 & 0 \\ 0 & 0 & 0 & 0 & 1 & 0 \\ 0 & 0 & 0 & 0 & 0 & 1 \end{pmatrix} \quad (14.22)$$

6576 Substitute $\varepsilon - \psi$ to ε in the R_{43} coefficient, when accounting for fringe field extent λ .

6577 14.4.2 Quadrupole

6578 Most of the time in beam lines and cyclic accelerators, guiding and focusing are
6579 separate functions, focusing is assured by quadrupoles, magnetic most frequently,
6580 possibly electrostatic at low energy. Quadrupoles are the optical lenses of charged
6581 particle beams, they ensure confinement of the beam in the vicinity of the optical
6582 axis.

6583 The field in quadrupole lenses results from hyperbolic equipotentials, $V = axy$.
6584 Pole profiles in quadrupole lenses follow these equipotentials, in a $2\pi/4$ -symmetrical
6585 arrangement for technological simplicity.

6586 14.4.2.1 Magnetic Quadrupole

6587 Magnetic quadrupoles are the optical lenses of high energy beams.

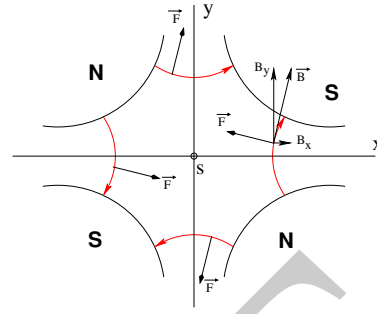
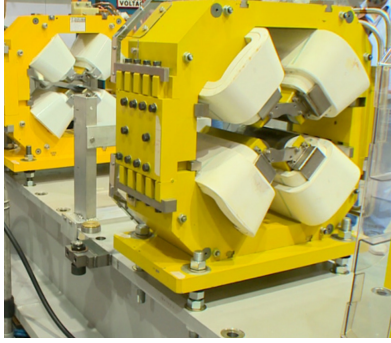


Fig. 14.8 Left: a quadrupole magnet [11]. Right: field lines and forces (assuming positive charges moving out of the page) over the cross section of an horizontally focusing / vertically defocusing quadrupole

6588 The theoretical field in a quadrupole can be derived from Eq. 14.9 for the scalar
6589 potential, with $n = 2$ which yields

$$V_2(X, Y, Z) = \mathcal{G}(X)YZ - \frac{\mathcal{G}''(X)}{12} (Y^2 + Z^2)YZ + \frac{\mathcal{G}^{(4)}(X)}{384} (Y^2 + Z^2)^2YZ - \dots \quad (14.23)$$

6590 and

$$B_X(X, Y, Z) = -\frac{\partial V_2}{\partial X} = \mathcal{G}'(X)YZ - \frac{\mathcal{G}'''(X)}{12} (Y^2 + Z^2)YZ + \dots \quad (14.24)$$

$$B_Y(X, Y, Z) = -\frac{\partial V_2}{\partial Y} = \mathcal{G}(X)Z - \frac{\mathcal{G}''(X)}{12} (3Y^2 + Z^2)Z + \dots \quad (14.25)$$

$$B_Z(X, Y, Z) = -\frac{\partial V_2}{\partial Z} = \mathcal{G}(X)Y - \frac{\mathcal{G}''(X)}{12} (Y^2 + 3Z^2)Y + \dots \quad (14.26)$$

6591 $\mathcal{G}(X)$ is given by Eq. 14.4 whereas

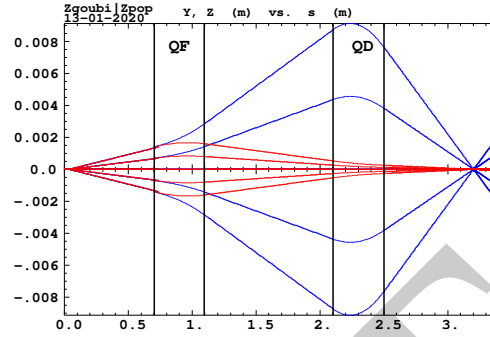
$$G_0 = \frac{B_0}{r_0} \quad \text{and} \quad K = G_0/B\rho \quad (14.27)$$

6592 define respectively the quadrupole gradient and strength, the latter relative to the
6593 rigidity $B\rho$. The quadrupole is horizontally focusing and vertically defocusing if
6594 $K > 0$, and the reverse if $K < 0$, this is illustrated in Fig. 14.9 which shows a doublet
6595 of quadrupoles with focusing strengths of opposite signs.

6596 *Linear approach*

6597 The first order transport matrix of a quadrupole with length L , gradient G and
6598 strength $K = G/B\rho$ writes

Fig. 14.9 Horizontal and vertical projections of particle trajectories across a stigmatic quadrupole doublet. The first quadrupole (QF) is horizontally focusing ($K > 0$; thus vertically defocusing), the second one (QD) has the reverse sign ($K < 0$)



$$T_{\text{quad}} = \begin{pmatrix} C_x & S_x & 0 & 0 & 0 & 0 \\ C'_x & S'_x & 0 & 0 & 0 & 0 \\ 0 & 0 & C_y & S_y & 0 & 0 \\ 0 & 0 & C'_y & S'_y & 0 & 0 \\ 0 & 0 & 0 & 0 & 1 & \frac{L}{\gamma^2} \\ 0 & 0 & 0 & 0 & 0 & 1 \end{pmatrix} \quad \text{with} \quad \begin{cases} C_x = \cos L\sqrt{K}; C'_x = \frac{dC_x}{dL} = -KS_x \\ S_x = \frac{1}{\sqrt{K}} \sin L\sqrt{K}; S'_x = \frac{dS_x}{dL} = C_x \\ C_y = \cosh L\sqrt{K}; C'_y = \frac{dC_y}{dL} = KS_y \\ S_y = \frac{1}{\sqrt{K}} \sinh L\sqrt{K}; S'_y = \frac{dS_y}{dL} = C_y \end{cases} \quad (14.28)$$

6599 $K > 0$ for a focusing quadrupole (by convention, in the (x, x') plane, thus defocusing
 6600 in the (y, y') plane). Permute the horizontal and vertical 2×2 sub-matrices in the
 6601 case of a *defocusing* quadrupole.

6602 14.4.2.2 Electrostatic Quadrupole

6603 The hypotheses are those of Sect. 2.2.2: paraxial motion, field normal to velocity,
 6604 etc. Take the notations of Eqs. 2.25, 2.26 for the field and potential, electrodes in
 6605 the horizontal and vertical planes (Fig. 2.14). Electrode potential is $\pm V/2$, pole tip
 6606 radius a , so that $K = -V/2a^2$ in Eq. 2.26. The equations of motion then write

$$\begin{cases} \frac{d^2x}{ds^2} + K_x x = 0 \\ \frac{d^2y}{ds^2} + K_y y = 0 \end{cases} \quad \text{with} \quad K_x = -K_y = \frac{-qV}{a^2 m v^2} = \pm \frac{V}{a^2} \underbrace{\frac{1}{|E\rho|}}_{\text{electrical rigidity}} \quad (14.29)$$

6607 With that $K = \frac{V}{a^2} \frac{1}{|E\rho|} = \frac{V}{a^2} \frac{1}{v(B\rho)}$ value ($(B\rho) = p/q$ is the particle magnetic
 6608 rigidity), the transport matrix is the same as for the magnetic quadrupole, Eq. 14.28.

6609 14.4.3 Solenoid

6610 Assume a solenoid magnet with (OX) its longitudinal axis, and revolution symmetry,
 6611 With $(O; X, r, \phi)$ cylindrical frame, radius r , and angle ϕ the coordinates in the X-
 6612 normal plane, $B_\phi(X, r, \phi) \equiv 0$. Take solenoid length L , mean coil radius r_0 and an
 6613 asymptotic field $B_0 = \mu_0 NI/L$ with $NI =$ number of ampere-Turns, $\mu_0 = 4\pi \times 10^{-7}$.
 6614 The asymptotic field value is defined by

$$\int_{-\infty}^{\infty} B_X(X, r < r_0) dX = \mu_0 NI = B_0 L \quad \text{independent of } r \quad (14.30)$$

6615 There is a variety of methods to compute the field vector $\mathbf{B}(X, r)$. Opting for one
 6616 in particular may be a matter of compromise between computing speed and field
 6617 modeling accuracy. A simple model is the on-axis field

$$B_X(X, r = 0) = \frac{B_0}{2} \left[\frac{L/2 - X}{\sqrt{(L/2 - X)^2 + r_0^2}} + \frac{L/2 + X}{\sqrt{(L/2 + X)^2 + r_0^2}} \right] \quad (14.31)$$

6618 with $X = r = 0$ taken at the center of the solenoid. This model assumes that the coil
 6619 thickness is small compared to its mean radius r_0 . The magnetic length comes out
 6620 to be

$$L_{\text{mag}} \equiv \frac{\int_{-\infty}^{\infty} B_X(X, r < r_0) dX}{B_X(X = r = 0)} = L \sqrt{1 + \frac{4r_0^2}{L^2}} > L \quad (14.32)$$

so satisfying

$$\text{on-axis } B_X(X = r = 0) = \frac{\mu_0 NI}{L \sqrt{1 + \frac{4r_0^2}{L^2}}} \xrightarrow{r_0 \ll XL} \frac{\mu_0 NI}{L}$$

6621 Maxwell's equations and Taylor expansions provide the off-axis field $\mathbf{B}(X, r) =$
 6622 $(B_X(X, r), B_r(X, r))$. One has in particular in the $r_0 \ll XL$ limit,

$$B_X(X, r) = \frac{\mu_0 NI}{L} \quad \text{and} \quad B_r(X, r) = \frac{-r}{2} \frac{dB_X}{dX} \quad (14.33)$$

6623 An other way to compute the field vector $\mathbf{B}(X, r)$ is the elliptic integrals technique
 6624 developed in [12], which constructs $B_X(X, r)$ and $B_r(X, r)$ from respectively

$$B_X(X, r) = \frac{\mu_0 NI}{4\pi} \frac{ck}{r} X \left[K + \frac{r_0 - r}{2r_0} (\Pi - K) \right] \quad (14.34)$$

$$B_r(X, r) = \mu_0 NI \frac{1}{k} \sqrt{\frac{r_0}{r}} \left[2(K - E) - k^2 K \right]$$

wherein K , E and Π are the three complete elliptic integrals, X is an X - and L -dependent form factor, and

$$k = 2\sqrt{r_0 r} / \sqrt{(r_0 + r)^2 + X^2}; \quad c = 2\sqrt{r_0 r} / (r_0 + r)$$

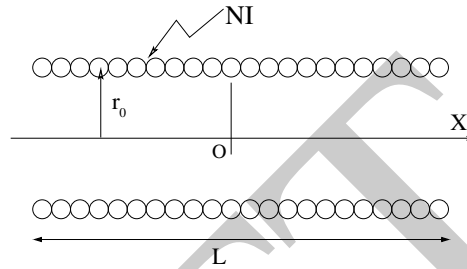


Fig. 14.10 A sketch of a solenoid, and quantities used to define it

6625

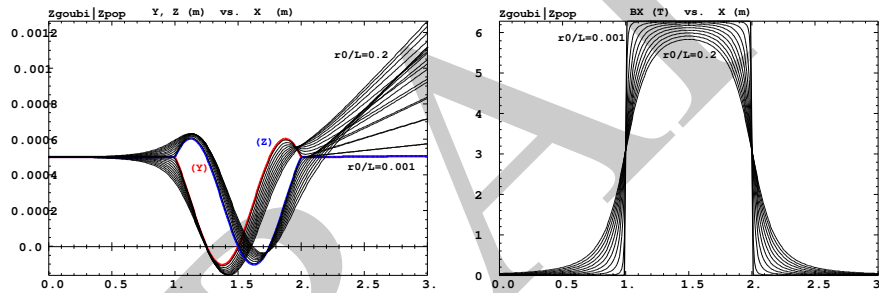


Fig. 14.11 Left: Horizontal (Y) and vertical (Z) projections of a particle trajectory across a $L = 1$ m solenoid, with additional 1 m extents upstream and downstream of the coil. The particle is launched with zero incidence, from transverse position $Y = Z = 0.5$ mm. Sample solenoid radius/length values in the range $0.001 \leq r_0/L \leq 0.2$ show that only for smallest $r_0/L = 0.001$ does the trajectory end with $Y = Z = 0.5$ mm and quasi-zero incidence (the thicker $Y(X)$ and $Z(X)$ curves), whereas greater r_0/L causes final $Y(X)$ and $Z(X)$ to be kicked away. Right: field $B_X(X, r)$ experienced along the trajectory for the various r_0/L values, the steep fall-off case is for $r_0/L = 0.001$.

6626

6627

6628

6629

6630

As an illustration, Fig. 14.11 displays a trajectory across a $L = 1$ m solenoid and its fringe field extents, and the field experienced along that trajectory, in the axial model of Eq. 14.31. In the paraxial approximation, a pitch requires a distance $l = 2\pi/K$, with $K = B_0/B\rho$ the solenoid strength, which is a condition satisfied here if the fringe field extent is short enough (r_0 is small enough).

6631 *Linear approach*

6632 The equations of motion write, to the first order in the coordinates, in respectively
6633 the central region (field B_s) and at the ends (at $s = s_{\text{EFB}}$),

$$\left\{ \begin{array}{l} x'' - K z' = 0 \\ z'' + K x' = 0 \end{array} \right. \quad \text{and} \quad \left\{ \begin{array}{l} x'' - \frac{K}{2} z \delta(s - s_{\text{EFB}}) = 0 \\ z'' + \frac{K}{2} x \delta(s - s_{\text{EFB}}) = 0 \end{array} \right. \quad (14.35)$$

6634 The first order transport matrix of a solenoid with length L writes

$$T_{\text{sol}} = \begin{pmatrix} C^2 & \frac{2}{K} SC & SC & \frac{2}{K} S^2 & 0 & 0 \\ -\frac{K}{2} SC & C^2 & -\frac{K}{2} S^2 & SC & 0 & 0 \\ -SC & -\frac{2}{K} S^2 & C^2 & \frac{2}{K} SC & 0 & 0 \\ \frac{K}{2} S^2 & -SC & -\frac{K}{2} SC & C^2 & 0 & 0 \\ 0 & 0 & 0 & 0 & 1 & \frac{L}{\gamma^2} \\ 0 & 0 & 0 & 0 & 0 & 1 \end{pmatrix} \quad \text{with} \quad \begin{cases} K = \frac{B_s}{B\rho} \\ C = \cos \frac{KL}{2} \\ S = \sin \frac{KL}{2} \end{cases} \quad (14.36)$$

6635 A solenoid rotates the decoupled axis longitudinally by an angle $\alpha = KL/2 =$
6636 $B_s L / 2B\rho$.

6637 14.5 Data Treatment Keywords

6638 14.5.1 Concentration Ellipse: FAISCEAU, FIT[2], MCOBJET, ...

6639 It is often useful to associate the projection of a particle bunch in the horizontal,
6640 vertical or longitudinal phase space with an *rms* phase space concentration ellipse
6641 (CE). Various keywords in `zgoubi` resort to concentration ellipses:

- 6642 - FAISCEAU for instance prints out, in `zgoubi.res`, CE parameters drawn from
- 6643 individual particle coordinates
- 6644 - random particle distributions by MCOBJET are defined using CE parameters.
- 6645 - ellipse parameters computed from CEs are possible constraints in FIT[2] pro-
- 6646 cedures.

6647 Transverse phase space graphs by `zpop` also compute CEs.

6648 The CE method is resorted to in various exercises, for instance for comparison
6649 of the ellipse parameters it gets from the *rms* matching of a bunch, with theoretical
6650 beam parameters, as derived from first order transport formalism or computed from
6651 rays by MATRIX, or TWISS.

6652 The method used in these various keywords and data treatment procedures is the
6653 following. Let $z_i(s)$, $z'_i(s)$ be the phase space coordinates of $i = 1, n$ particles in a set
6654 observed at some azimuth s along a beam line or in a ring. The second moments of
6655 the particle distribution are

$$\begin{aligned}\overline{z^2}(s) &= \frac{1}{n} \sum_{i=1}^n (z_i(s) - \overline{z}(s))^2 \\ \overline{zz'}(s) &= \frac{1}{n} \sum_{i=1}^n (z_i(s) - \overline{z}(s))(z'_i(s) - \overline{z'}(s)) \\ \overline{z'^2}(s) &= \frac{1}{n} \sum_{i=1}^n (z'_i(s) - \overline{z'}(s))^2\end{aligned}\quad (14.37)$$

6656 From these, a concentration ellipse (CE) is drawn, encompassing a surface $S_z(s)$,
6657 with equation

$$\gamma_c(s)z^2 + 2\alpha_c(s)zz' + \beta_c(s)z'^2 = S_z(s)/\pi \quad (14.38)$$

6658 Noting $\Delta = \overline{z^2}(s)\overline{z'^2}(s) - \overline{zz'}^2(s)$, the ellipse parameters write

$$\gamma_c(s) = \frac{\overline{z'^2}(s)}{\sqrt{\Delta}}, \quad \alpha_c(s) = -\frac{\overline{zz'}(s)}{\sqrt{\Delta}}, \quad \beta_c(s) = \frac{\overline{z^2}(s)}{\sqrt{\Delta}}, \quad S_z(s) = 4\pi\sqrt{\Delta} \quad (14.39)$$

6659 With these conventions, the *rms* values of the z and z' projected densities satisfy

$$\sigma_z = \sqrt{\beta_z \frac{S_z}{\pi}} \quad \text{and} \quad \sigma_{z'} = \sqrt{\gamma_z \frac{S_z}{\pi}} \quad (14.40)$$

6660 14.5.2 Transport Coefficients: MATRIX, OPTICS, TWISS, etc.

6661 Zgoubi does not know about matrix transport, it does not define optical elements
6662 by a transport matrix, it defines them by electrostatic and/or magnetic fields in
6663 space (and time possibly). Well, except for a couple of optical elements, for instance
6664 TRANSMAT, which pushes particle coordinates using a matrix, or SEPARA, an
6665 analytical mapping through a Wien filter. Zgoubi does not transport particles using
6666 matrix products either, it does that by numerical integration of Lorentz force equation.

6667 However it is often useful to dispose of a matrix representation of an optical
6668 element, of the transport matrix of a beam line, or the first or second order one-turn
6669 matrix of a ring accelerator. It may also be useful to compute the beam matrix and its
6670 transport. Several commands in zgoubi perform the necessary particle coordinates
6671 treatment to derive these informations. Examples are MATRIX: computation of
6672 matrix transport coefficients up to 3rd order, from initial and current coordinates of
6673 a particle sample. OPTICS transports a beam matrix, given its initial value using
6674 OBJET[KOBJ=5.1] (see Sect. 14.5.2.2). TWISS derives a periodic beam matrix
6675 from a 1-turn mapping of a periodic sequence, and transports it from end to end so
6676 generating the optical functions along the sequence (Sects. 14.5.2.2, 14.5.2.3).

6677 These capabilities are used the exercises. It may be required for instance to
6678 compare transport coefficients derived from raytracing, with the matrix model of the
6679 optical element(s) concerned. Or to compute a periodic beam matrix in a periodic

6680 optical sequence, this is how betatron functions are produced, often for the mere
 6681 purpose of comparisons with matrix code outcomes, or with expectations from
 6682 analytical models.

6683 14.5.2.1 Coordinate Transport

6684 In the Gauss approximation (*i.e.*, with θ the angle of a trajectory to the reference
 6685 axis, $\sin \theta \sim \theta$), particles follow paths which can be described with simple functions:
 6686 parabolic, sinusoidal or hyperbolic. A consequence is that a string of optical elements,
 6687 and coordinate transport through the latter, can be handled with a simple mathematics
 6688 toolbox. Taylor expansion (also known as transport) techniques are part of it, whereby
 6689 a coordinate excursion v_{2i} (with index $i = 1 \rightarrow 6$ standing for $x, x', y, y', \delta s$ or
 6690 $\delta p/p$) from some reference trajectory at a location s_2 along the line is obtained from
 6691 the excursions v_{1i} at an upstream location s_1 , via

$$v_{2i} = \sum_{j=1}^6 R_{ij} v_{1j} + \sum_{j,k=1}^6 T_{ijk} v_{1j} v_{1k} + \sum_{j,k,l=1}^6 v_{1ijkl} v_{1j} v_{1k} v_{1l} + \dots \quad (14.41)$$

6692 This Taylor development can be written under matrix form, for instance to the
 6693 first order in the coordinates, for non-coupled motion,

$$\begin{pmatrix} x \\ x' \\ y \\ y' \\ \delta s \\ \delta p/p \end{pmatrix}_2 = \begin{pmatrix} T_{11} & T_{12} & 0 & 0 & 0 & T_{16} \\ T_{21} & T_{22} & 0 & 0 & 0 & T_{26} \\ 0 & 0 & T_{33} & T_{34} & 0 & T_{36} \\ 0 & 0 & T_{43} & T_{44} & 0 & T_{46} \\ 0 & 0 & 0 & 0 & T_{55} & T_{56} \\ 0 & 0 & 0 & 0 & T_{65} & T_{66} \end{pmatrix} \begin{pmatrix} x \\ x' \\ y \\ y' \\ \delta s \\ \delta p/p \end{pmatrix}_1 = T(s_2 \leftarrow s_1) \begin{pmatrix} x \\ x' \\ y \\ y' \\ \delta s \\ \delta p/p \end{pmatrix}_1 \quad (14.42)$$

6694 These are the objects keywords as MATRIX [1, *cf.* Sect. 6.5] and OPTICS [1,
 6695 *cf.* Sect. 6.4] compute: the values of the transport coefficients, or transport matrices
 6696 to first and high order, are drawn from particle coordinates. Transport matrices of
 6697 common optical elements (drift, dipole, quadrupole, etc., magnetic or electrostatic),
 6698 are resorted to in the exercises for comparison with their matrix representation.

6699 14.5.2.2 Beam Matrix

6700 OPTICS and TWISS keywords cause the transport of a beam matrix. The former
 6701 requires an initial matrix: it is provided as part of the initial object definition, by
 6702 OBJET. The latter derives a periodic beam matrix from initial and final coordinates
 6703 resulting from raytracing throughout an optical sequence. Basic principles are re-
 6704 called here, This is the way it works in zgoubi, and in addition they are resorted to
 6705 in the exercises.

6706 In the linear approximation, the transverse phase space ellipse associated with a
 6707 particle distribution (for instance, the concentration ellipse, Sect. 14.5.1) is written
 6708 (with z standing for indifferently x or y)

$$\gamma_z(s)z^2 + 2\alpha_z(s)zz' + \beta_z(s)z'^2 = \frac{\varepsilon_z}{\pi} \quad (14.43)$$

6709 in which the ellipse parameters

$$\beta_z(s), \alpha_z(s) = -\frac{1}{2} \frac{d\beta_z}{ds}, \gamma_z(s) = \frac{1 + \alpha^2}{\beta_z} \quad (14.44)$$

6710 are functions of the azimuth s along the optical sequence. The surface ε_z of the ellipse
 6711 is an invariant if the beam travels in magnetic fields, however field non-linearities,
 6712 phase space dilution, etc. may distort the distribution and change the surface of its
 6713 *rms* matching concentration ellipse. In the presence of acceleration or deceleration
 6714 the invariant quantity is $\beta\gamma\varepsilon_z$ instead, with $\beta = v/c$ and γ the Lorentz relativistic
 6715 factor.

6716 The ellipse Eq. 14.43 can be written under the matrix form

$$\mathbf{1} = \tilde{T} \sigma_z^{-1} T \quad (14.45)$$

6717 with σ_z the beam matrix:

$$\sigma_z = \frac{\varepsilon_z}{\pi} \begin{pmatrix} \beta_z & -\alpha_z \\ -\alpha_z & \gamma_z \end{pmatrix} \quad (14.46)$$

6718 The ellipse parameters can be transported from s_1 to s_2 using

$$\sigma_{z,2} = T \sigma_{z,1} \tilde{T} \quad (14.47)$$

6719 with $T = T(s_2 \leftarrow s_1)$ the transport matrix (Eq. 14.42) and \tilde{T} its transposed. This can
 6720 also be written under the form

$$\begin{pmatrix} \beta_z \\ \alpha_z \\ \gamma_z \end{pmatrix}_2 = \begin{pmatrix} T_{11}^2 & -2T_{11}T_{12} & T_{12}^2 \\ -T_{11}T_{21} & T_{21}T_{12} + T_{11}T_{22} & -T_{12}T_{22} \\ T_{21}^2 & -2T_{21}T_{22} & T_{22}^2 \end{pmatrix}_{s_2 \leftarrow s_1} \begin{pmatrix} \beta_z \\ \alpha_z \\ \gamma_z \end{pmatrix}_1 \quad (14.48)$$

6721 (subscripts 1, 2 normally hold for horizontal plane motion, $z = x$: change to 3, 4
 6722 for vertical motion, $z = y$). This beam matrix formalism can be extended to the
 6723 longitudinal phase space and coordinates $(\delta s, \delta p/p)$, a 6×6 beam matrix can be
 6724 defined,

$$\sigma = \begin{pmatrix} \sigma_{11} & \sigma_{12} & 0 & 0 & 0 & \sigma_{16} \\ \sigma_{21} & \sigma_{22} & 0 & 0 & 0 & \sigma_{26} \\ 0 & 0 & \sigma_{33} & \sigma_{34} & 0 & \sigma_{36} \\ 0 & 0 & \sigma_{43} & \sigma_{44} & 0 & \sigma_{46} \\ 0 & 0 & 0 & 0 & \sigma_{55} & \sigma_{56} \\ 0 & 0 & 0 & 0 & \sigma_{65} & \sigma_{66} \end{pmatrix} \quad (14.49)$$

6725 This can be generalized to non-zero anti-diagonal coupling terms, if motions are
6726 coupled.

6727 14.5.2.3 Periodic Structures

6728 In the hypothesis of an S - periodic structure: a long beam line with repeating pattern,
6729 a cyclic accelerator, transverse motion stability requires the transport matrix over a
6730 period, from s to $s + S$ to satisfy

$$[T_{ij}](s + S \leftarrow s) = I \cos \mu + J \sin \mu \quad (14.50)$$

6731 where $\mu = \int_{(S)} ds/\beta$ is the betatron phase advance over the period (independent of
6732 the origin),

$$I = \begin{pmatrix} 1 & 0 \\ 0 & 1 \end{pmatrix} \text{ is the identity matrix, } J = \begin{pmatrix} \alpha_z(s) & \beta_z(s) \\ -\gamma_z(s) & -\alpha_z(s) \end{pmatrix} \text{ (and } J^2 = -I) \quad (14.51)$$

6733 14.6 Exercises

6734 14.1 Magnetic Sector Dipole

6735 Solution: page 605.

6736 (a) Simulate a $\rho = 1$ m radius, $\alpha = 60$ degree sector dipole with $n=-0.6$ field
6737 index, in both cases of hard edge and of soft fall-off fringe field model. Find the
6738 reference arc, such that $\int_{\text{arc}} B ds = BL$ with L the arc length in the hard-edge model
6739 and B the field along that arc.

6740 Make sure the reference arc has the expected length.

6741 Produce the field along the reference arc, for a few different values of the fringe-
6742 field extent.

6743 (b) A possible check of the first order: OBJET[KOBJ=5], MATRIX[IORD=1,IFOC=0]
6744 can be used to compute the transport matrix from the rays. Compare what it gives
6745 with theory.

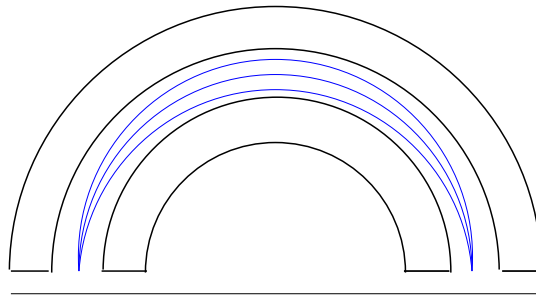


Fig. 14.12 Focusing by a 180 deg dipole

6746 (c) Consider a 180 deg wedge sector with uniform field. Show the well known
6747 geometrical property (cf. Sect. 3.2.2): this bend re-focuses at its exit EFB a diverging
6748 beam launched from the entrance EFB along the reference radius (Fig. 14.12).

6749 Test the convergence of the numerical solution versus integration step size.

6750 (d) Transport a proton along the reference axis, injected with its spin tangent to
6751 the axis. Compare spin rotation with theory.

6752 Test the convergence of the numerical solution versus integration step size.

6753 14.2 Solenoid

6754 Solution: page 609.

6755 An introduction to SOLENOID.

6756 (a) Reproduce Fig. 14.11. Use both fields models of Eqs. 14.31, 14.34 and compare
6757 their outcomes, including the first order paraxial transport matrices, higher order as
6758 well (computed from in and out trajectory coordinates).

6759 (b) Compare final coordinates in (a) with outcomes from the first order transport
6760 formalism (Sect. 14.4.3).

6761 (c) Make a 1-dimensional (on-axis) field map of a $r_0 = 10$ cm, $L = 1$ m solenoid
6762 (namely, a map $B_{X,i}(X_i)$ of the field at the nodes of a X-mesh with mesh size
6763 $X_{i+1} - X_i$). Reproduce the trajectory in (a) (case $r_0 = 10$ cm) using that field map,
6764 with the keyword BREVOL. Check the convergence of the final particle coordinates,
6765 using the field map, depending on the mesh size.

6766 References

- 6767 1. Méot, F.: Zgoubi Users' Guide.
6768 <https://www.osti.gov/biblio/1062013-zgoubi-users-guide> Sourceforge latest version:
6769 <https://sourceforge.net/p/zgoubi/code/HEAD/tree/trunk/guide/Zgoubi.pdf>
- 6770 2. The AGS at the Brookhaven National Laboratory: <https://www.bnl.gov/rhic/AGS.asp>
- 6771 3. The CERN PS: <https://home.cern/science/accelerators/proton-synchrotron>
- 6772 4. Volk, James T.: Experiences with permanent magnets at the Fermilab recycler ring.
6773 James T Volk 2011 JINST6 T08003. <https://iopscience.iop.org/article/10.1088/1748-0221/6/08/T08003/pdf>
- 6774 5. Duthheil, Y.: A model of the AGS based on stepwise ray-tracing through the measured field maps
6775 of the main magnets. Proceedings of IPAC2012, New Orleans, Louisiana, USA, TUPPC101,
6776 1395-1399.
6777 <https://accelconf.web.cern.ch/IPAC2012/papers/tuppc101.pdf>
- 6778 Méot, et al.: Modeling of the AGS using zgoubi - status. Proceedings of IPAC2012, New
6779 Orleans, Louisiana, USA, MOPPC024, 181-183.
6780 <https://accelconf.web.cern.ch/IPAC2012/papers/moppc024.pdf>
- 6781 6. Enge, H. A.: Deflecting magnets. In: Focusing of Charged Particles, ed. A. Septier, Vol. II,
6782 pp. 203-264, Academic Press Inc., 1967
- 6783 7. Thern, R. E., Bleser, E.: The dipole fields of the AGS main magnets, BNL-104840-2014-
6784 TECH, 1/26/1996.
6785 <https://technotes.bnl.gov/PDF?publicationId=31175>
- 6786 8. Méot, F., Ahrens L., Brown, K., et al.: A model of polarized-beam AGS in
6787 the ray-tracing code Zgoubi. BNL-112453-2016-TECH, C-A/AP/566 (July 2016).
6788 <https://technotes.bnl.gov/PDF?publicationId=40470>

- 6790 9. Méot, F., Lemuet, F.: Developments in the ray-tracing code Zgoubi for 6-D multiturn tracking
6791 in FFAG rings. NIM A 547 (2005) 638-651.
- 6792 10. Leleux, G.: Accélérateurs Circulaires. Lectures at the Institut National des Sciences et Tech-
6793 niques du Nucléaire, CEA Saclay (July 1978), unpublished
- 6794 11. Credit: Brookhaven National Laboratory.
6795 <https://www.flickr.com/photos/brookhavenlab/8495311598/in/album-72157611796003039/>
- 6796 12. Garrett, M.W.: Calculation of fields [...] by elliptic integrals. In: J. Appl. Phys., 34, 9, Sept. 1963

DRAFT